International Journal of Control, Automation and Systems 17(X) (2019) 1-11
http://dx.doi.org/10.1007/s12555-019-0239-6
ISSN:1598-6446 eISSN:2005-4092
http://www.springer.com/12555

Medical Microrobot - Wireless Manipulation of a Drug Delivery Carrier through an External Ultrasonic Actuation: Preliminary Results

Han-Sol Lee, Gwangjun Go, Eunpyo Choi, Byungjeon Kang*, Jong-Oh Park*, and Chang-Sei Kim*

Abstract: To achieve precise and untethered clinical therapeutics, microrobots have been widely researched. However, because conventional microrobot actuation is based on magnetic forces generated by a magnetic field and magnetic particles, unexpected side effects caused by additional magnetic ingredients could induce clinical safety issues. In this paper, as an alternative to an untethered actuator, we present a novel ultrasonic actuation mechanism that enables drug particle/cell manipulation and micro/nano-robot actuation in clinical biology and medicine. Firstly, characteristics of the acoustic field in the vessel mimic circular tube, formed from particles emerging through a submerged ultrasonic transducer, are mathematically analyzed and modeled. Thereafter, a control method is proposed for trapping and moving the micro-particles by using acoustic radiation force (ARF) in a standing wave of a tangential standing wave. The feasibility of the proposed method could be demonstrated with the help of experiments conducted using a single transducer with a resonance frequency of 950 kHz and a motorized linear stage, which were used in a water tank. The micro-particles in the tube were trapped via ultrasound and the position of the micro-particles could be controlled by frequency manipulation of the transducer and motor control. This study shows that ultrasonic manipulation can be used for specific applications, such as the operation of a micro robot inserted in a peripheral blood vessel and targeted for drug delivery.

Keywords: Drug delivery, medical microrobot,ultrasonic actuation, ultrasound, wireless actuation.

1. INTRODUCTION

Target-oriented clinical treatment methods based on micro/nano robots have been widely researched in the recent past [1]. Because of the untethered external actuation ability, the microrobot is able to move inside a human body to achieve accurate diagnosis and therapeutics as a distinguished mechanism from the conventional medical surgical robot [2]. Moreover, safe and minimally invasive treatment can be performed by the microrobot, thereby ensuring low risk of infection and internal injuries through vessels. Here, blood vessels are considered as both, a main route to maneuver a therapeutic agency towards the target region and a cause of cardiovascular disease. In the case of peripheral vascular disease, drugs can slow the progression of the disease and alleviate the symptoms. However, precise drug delivery to the target site is limited owing to circulation in the human body where drugs are diffused and moved inside the body.

The purpose of this study is to develop a target oriented untethered drug delivery system by using micro/nano robots that are injected into peripheral blood vessels. These blood vessels are thought to be body circulators in the form of circular tubes, as depicted in Fig. 1. In previous studies, the micro/nano robots were mainly driven by an electro-magnetic actuation system (EMA) [3–5]. Although the EMA was capable of providing a powerful and feasible actuation force and steering torque, it has several drawbacks, such as low efficiency of collection and target-

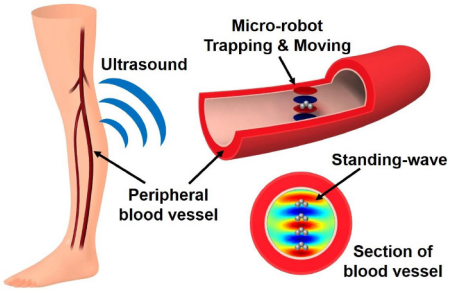

Fig. 1. The conceptual images of research.

Manuscript received April 1, 2019; revised August 18, 2019; accepted August 25, 2019. Recommended by Editor Doo Yong Lee. This research was supported by a grant of the Korea Health Technology Development R&D Project through the Korea Health Industry Development Institute (KHIDI), funded by the Ministry of Health & Welfare, Republic of Korea (grant number: HI19C0642).

Han-Sol Lee, Gwangjun Go, Eunpyo Choi, Jong-Oh Park, and Chang-Sei Kim are with School of Mechanical Engineering, Chonnam National University, 77, Yongbong-ro, Gwangju 61186, Korea (e-mails: hansol3607@gmail.com, {gwangjun124, eunpyochoi, jop, ckim}@jnu.ac.kr). Byungjeon Kang is with Korea Institute of Medical Microrobotics, 43-26, Cheomdangwagi-ro 208-beon-gil, Buk-gu, Gwangju 61011, Korea (e-mail: bjkang8204@jnu.ac.kr).
* Corresponding authors.

ing, relatively large equipment size, and power consumption.

An ultrasound can be used as an alternative for wireless actuation for a medical microrobot, since it's utilization offers several advantages. Firstly, it can generate acoustic radiation forces within a particular fluid medium to trap and manipulate particles [6]. Secondly, owing to its permeability, it can penetrate the medium, such as the skin of the human body and can access the internal tissues and blood vessels non-invasively. Thirdly, it causes very little damage to the soft target structure and target tissue surroundings. Fourth, the device is light weight, thus enabling hand-held manipulation. The final advantage is that ultrasound can drive and activate a wide range of particles from living cells to micro-structures with various components [7]. Therefore, ultrasound based mani-pulation techniques have been proposed for usage in non-contact operations for driving or handling drug carriers, regenerative robots, micro-organisms and medical micro/nano robots [8–10].

Several ultrasound actuation devices have been proposed in previous researches. For phase [7, 11, 12] or frequency control [8, 13] of standing waves, transducer arrays are used by placing them opposite each other on a two-dimensional plane. Another system showed an ultrasound actuation system that trapped particles and facilitated their movement through the transducer array in the chamber [14, 15]. In the recent past, a system has been studied in which multiple transducers are arrayed and then placed opposite each other in order to create standing wave fields so that the particles could be trapped and manipulated [16, 17]. Furthermore, studies of applying acoustic vortex [18] or electro-magnetic field [19, 20] to the ultrasonic transducer array system have been conducted. However, when these systems were used in practice, the ultrasonic waves were disturbed by the component having an acoustic impedance much higher than the tissues in the human body, like the bone. The resulting acoustic field produced in the body did not yield practical results. To tackle this, uni-directional manipulation systems were developed, such as a uni-directional array of ultrasonic transducers in the air [21, 22] and an acoustic beam formed by acoustic lens or transducer structural factors [6, 23]. These methods could avoid certain obstacles between the system and the target structures, and were more effective than the conventional manipulation systems, in terms of downsizing the system and application utilization.

However, particle manipulation using a transducer array system is generally operated in open air, which is generally less affected by acoustic streaming than water. Also, trapping systems utilizing lenses have limitations, such as multi-degree-of-freedom driving.

In this paper, we present a novel methodology for acoustic trapping and operation of micro-particles for the purpose of developing a precise active drug delivery system. It proceeds with the generation of an acoustic radiation force, with the help of an ultrasonic transducer, in the standing wave in the acoustic range formed. Specifically, this is accomplished by manipulating the z-axis position of the pressure node by controlling the frequency of the transducer, moving the y-axis of the focus area through the motorizing stage, and driving the micro-particles present in the tube. The proposed method is advantageous in that, it does not require placement of additional reflectors or transducers in the opposite direction. It forms a standing wave through the reflection of the ultrasound due to change in the media such as water or tube wall, which allows particle trapping and precise position control. Fig. 2 shows the overall system design and control mechanism of particle manipulation. A single ultrasonic transducer is sufficient to control the position of micro-particles in the z-direction through changes in frequency, and the motorization method is suitable for allowing micro-particles to follow the tube. These two ultrasonic actuation methods are shown in Fig. 2(b). Each method has been studied and various movements of the particles have been implemented by applying them.

In Section 2 of this paper, the acoustic field and the characteristics of the fluid such as acoustic potential, pressure nodes, and anti-nodes are analyzed by simulation

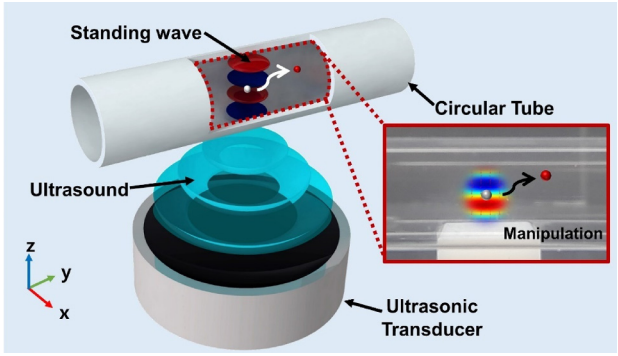

(a)

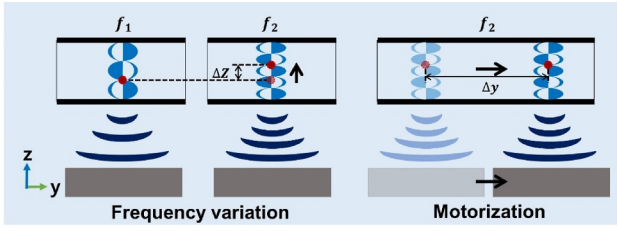

(b)

Fig. 2. (a) Illustration of the ultrasonic actuation system that can generate a standing wave in a circular tube and drive micro-particles using it. (b) Mechanism of micro-particle actuation through ultrasound frequency control and motorization at the center inside the tube.

and experiment according to ultrasound frequency change. Section 3 provides controller design for the ultrasonic based particle manipulation with automatic path tracking. *In-vitro* experimental results to verify the feasibility of the proposed method are shown in Section 4. This paper concludes with discussions on the research in Section 5.

2. ACOUSTIC FORCE MODELING

2.1. Acoustic radiation force

When the acoustic field is formed through the acoustic waves, the movement of the spherical particles existing in the interior is described by the following equations [7, 22, 24]:

$$m\ddot{z} = F_g + F_{rad} + F_{drag} + F_{buoyancy}, \tag{1}$$

where the coordinate of z is defined for gravity directional motion, m is the mass of the spherical particle, and F_g is the gravitational force acting on the particle. Also, F_{rad} is the acoustic radiation force, F_{drag} is the fluid drag force, and $F_{buoyancy}$ is the buoyant force. In the above equation, the force components affecting the particles are F_{rad} and F_{drag}.

The most dominant force used to manipulate particles present in the acoustic region is the acoustic radiation force (ARF). When an acoustic radiation force acts on the spherical particles in the acoustic field, it can be calculated from the equation related to the gradient of Gor'kov potential [25–28].

$$F_{rad} = -\nabla U_{rad}. \tag{2}$$

The Gor'kov potential equation consists of the acoustic pressure and velocity terms, and is given by:

$$U_{rad} = \frac{4\pi}{3}a^3\left[f_1\frac{1}{2}\kappa_0\left\langle p_1^2\right\rangle - f_2\frac{3}{4}\rho_0\left\langle v_1^2\right\rangle\right], \tag{3}$$

$$f_1(\widetilde{\kappa}) = 1-\widetilde{\kappa},\ \ \widetilde{\kappa} = \frac{\kappa_p}{\kappa_0}, \tag{4}$$

$$f_2(\widetilde{\rho}) = \frac{2(\widetilde{\rho}-1)}{2\widetilde{\rho}+1},\ \ \widetilde{\rho} = \frac{\rho_p}{\rho_0}, \tag{5}$$

where p_1 is the acoustic pressure in the medium and v_1 is the velocity of fluid obtained from Navier-Stokes first order equation. a is the radius of the spherical particle, κ_p and κ_0 are the compressibility of the particle and fluid, and ρ_p and ρ_0 are the density of the particle and fluid, respectively. Also, f_1 is the monopole coefficient and f_2 is the dipole coefficient, which are computed as the value for density and compressibility of target particle and fluid medium, respectively. Finally, since $\langle\cdot\rangle$ is time averaged value, hence, $\langle p\rangle$ and $\langle v\rangle$ are the time averaged acoustic pressure and velocity of the fluid.

When a standing wave is formed in the acoustic field, pressure nodes and anti-nodes are formed at half-wavelength intervals in the area. If a rigid particle with a spherical model exists in this region, the particle is captured by each pressure node located in the standing wave by the acoustic radiation force. If the particle's compressibility is smaller than that of the sound field, such as water droplets, the ARF will act in a direction opposite to the existing one and will be captured by the anti-node [15].

Here, the basic assumption is that the particle size should be much smaller than the wavelength of the ultrasonic wave, according to the Rayleigh regime. In order to trap particles in a stable manner in the standing wave region, they must be placed at pressure nodes that occur at half-wave intervals and receive an acoustic radiation force from a region of high pressure. However, if the particle is larger than the wavelength, the above conditions do not apply and stable trapping is also impossible. In this study, we used a spherical scaffold (drug delivery carrier) with a diameter of 300 μm. The frequency of the ultrasound for levitation motion control is approximately 800-1500 kHz, whereas the ultrasonic wavelength inside the medium (water) is approximately 1 mm or more. As a result, the ultrasound frequency is approximately 950 kHz (resonant frequency of transducer) and corresponds to a wavelength of approximately 1.6 mm (minimum 1 mm), which validates the basic theoretical assumption that the radius of the particle is much smaller than the wavelength in theory.

2.2. Acoustic streaming

The Navier-Stokes and continuity equation, and the linear equation obtained by linearization using the perturbation approximation, is the acoustic pressure and velocity of the acoustic radiation force mentioned above. Through the quadratic equation, we derive the streaming velocity of the acoustic region.

In general, the Stokes drag force is given by [29]:

$$F_{drag} = 6\pi\mu a(\langle v_2\rangle - v), \tag{6}$$

where μ is the dynamic viscosity of fluid, a is the radius of the spherical particle, v_2 is the streaming velocity, and v is the particle's velocity, respectively.

Here, the drag force induced by nonlinear acoustic streaming plays an equally important role as the acoustic radiation force, which is said to be the most dominant in the acoustic field for trapping and maintaining the particles in the fluids in a stable manner. Therefore, it is possible to conceive a system capable of driving by trapping the micro-particles at the node and changing the position of the node. This can be induced by a change in the ultrasonic wave by using the acoustic radiation force and fluid drag force by fluid streaming, which represents the physical force generated in the acoustic field.

2.3. Simulation of acoustic field

Fig. 3 shows the physical characteristics of the model performed by simulation. Since the micro-particles

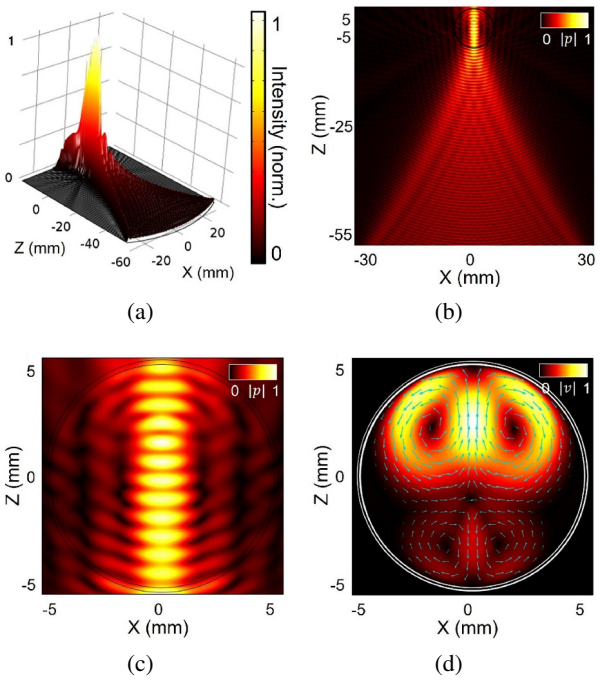

Fig. 3. (a) The normalized intensity of ultrasonic transducer at 950 kHz. (b), (c) The simulated results of pressure field when frequency is (c) 950 kHz. (d) Simulated results of acoustic streaming and velocity component when the frequency is 950 kHz.

present in the acoustic region must be precisely controlled, it is necessary to understand the physical characteristics of the region of interest. For the analysis, we identified the characteristics through modeling via a COMSOL simulation. In the model, a transducer with a concave curvature on the generating surface forms the focus of the acoustic beam. The focus was located at the center of a 10 mm diameter tube inserted in the water.

When an acoustic beam is formed through a transducer, as shown in Fig. 3(a), a focal zone is created at a position 58 mm from the transducer. The intensity in this space is highly formed owing to the focusing of the acoustic wave propagating perpendicular to the generating surface of the transducer. When the focal zone is located at the center of the tube, standing waves are formed owing to the nature of the ultrasound. In this case, the standing wave is generated by the superposition of the traveling wave transmitted through the tube and the reflected wave generated by colliding with the tube wall reflector.

Fig. 3(b) shows the characteristics of the whole fluid area, from the ultrasound generator to the tube, and (c) is the enlargement of the in-tube region, which is the focal zone. These figures show the pressure distribution of the acoustic field inside the tube according to the frequency settings of 950 kHz. When applying the above theory, it can be seen that a region formed with high pressure and a region formed with low pressure in the z-direction form a layer together. This layer corresponds to the antinodes formed in sequence having nodes with many vibrations and nodes with few vibrations, respectively, resulting in superposition of waves, and thereby providing a standing wave. Further, Fig. 3(d) shows the distribution of acoustic streaming formed by the ultrasound generated at 950 kHz. The brightest part depicts the faster streaming, the darker part represents the lower streaming speed, and the arrow shows the direction and magnitude of the speed. In the Fig. 3(d), the flow spreading to the left and right tends to converge at the center of the tube. This is because ultrasonic waves generated from the transducer are reflected onto the tube wall or repeatedly circulated around the round wall. The drag force, which is proportional to the streaming velocity, acts in the direction of the pressure node at the center of the tube. As a result, particles can be trapped within the region of interest by the acoustic radiation force owing to acoustic potential, drag force by streaming, gravity and buoyancy acting on the particles.

3. CONTROLLER DESIGN

The position controller is designed by utilizing ultrasonic characteristics obtained from simulation and experiments. The hardware is composed of an ultrasonic transducer for levitation and x-y directional motorized devices for translation. The composite position control will be explained in this section. Fig. 4 depicts a block diagram of the whole composite control system used in this study.

3.1. Levitation

In order to move the particle in the z-direction, we must be able to control the position of the nodes of the standing wave through the frequency change. As shown in Fig. 5, the positions of the nodes generated at the set frequency and the positions of adjacent nodes are found to behave linearly. In this case, nodes 1-7 are all pressure nodes that

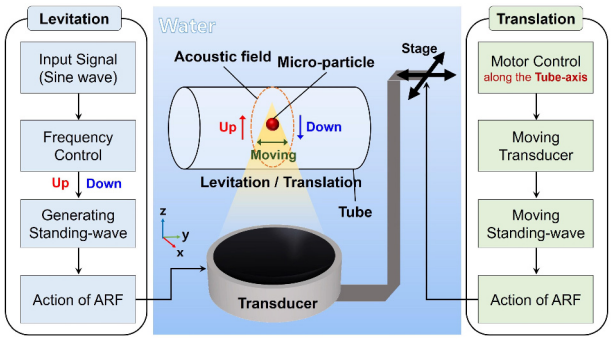

Fig. 4. Simplified illustrations of the mechanism of microparticle manipulation through frequency variation.

can be generated at 600 kHz. It can also be seen that when frequency increases continuously, the particle moves up slightly in the positive z-direction. Using these aspects, we can derive a position controller for the trapped particle in the node by continuously changing the frequency and controlling the position of the node. In this way, if micro-particles are trapped at a particular node in the standing wave of the set frequency, its position can be controlled through continuous frequency changes. More precisely, given a continuous frequency change, the trapping point under the acoustic radiation force follows the position of the changing nodes. At the new trapping point, the particles are collected again. Fig. 5 consists of a look-up table for levitation. It shows that the particles captured at the corresponding points of each node can levitate through continuous frequency changes. This simulation result is expressed through a curve fitting method in the following equation:

$$P_n = p(1) + p(2)n + p(3)f + p(4)nf + p(5)f^2, \quad (7)$$

where P_n is a function indicating the location of nodes according to node number and frequency, n is the node number 1-7 of nodes in Fig. 5, f is the frequency in kHz, and $p = [2.238, 1.542, 0.852, -0.433, -0.262]$.

3.2. Translational motion

The translation motion is implemented with the help of an additional x-y planar stage as shown in Fig. 4. When a standing wave of a certain frequency is formed in the tube from an ultrasonic transducer and particles are trapped, the movement of the transducer through the stage changes the position of the focal zone. As a result, the position of the standing wave field moves along the focal zone. In this case, the particles are directed towards the changed area.

However, the direction of the translational motion is limited to only the axial direction of the tube, owing to the drag force that acts in the axial direction owing to the acoustic streaming occurring in the tube. This aspect needs to be understood in future researches.

3.3. Composite feedback control

Fig. 6 shows a block diagram of automatic path tracking control of the particles. First, the images of a particle inside the tube are captured by the camera that identifies the current position and computes differences with respect to the desired position. Δy and Δz are the distances between the current position and the desired position of the micro-particle. According to the generated position difference, the particle position is controlled by the frequency variations in the ultrasonic transducer and the motor control in x-y stage. Here, f is the frequency variation for manipulating the micro-particle up or down in the z-direction and θ is the control value of the motorized stage. Finally, the data of the difference between the current and the desired position is fed back through the real-time image of the disposed camera and is controlled so as to follow the desired path continuously. In order to design a controller, we derive a system model based on the open loop dynamic behavior in simulations and experiments. The z- directional position (gravity direction) and y- directional position of the particles inside the tube can be expressed as follows:

$$P_{oz} = g_z(P_{iz},\ P_n), \quad (8)$$

$$P_{oy} = g_y(P_{iy},\ i_{stage}) = e^{-\tau s}\, P_{iy}\, i_{stage}, \quad (9)$$

where P_{oz} and P_{oy} are the output position of the particle along the z- and y-axis, respectively. g is a plant function describing the nonlinear dynamics of particle motion obtained by experiments. The behavior of (8) is modeled as fitted polynomial as depicted in the lower panel of Fig. 5 and (9) is assumed as a pure delay function. Function g

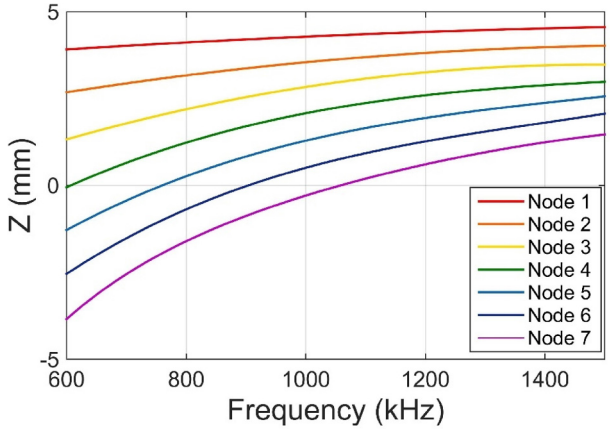

Fig. 5. Simulated results for the position change of each node when frequency is changed from 600 kHz to 1500 kHz.

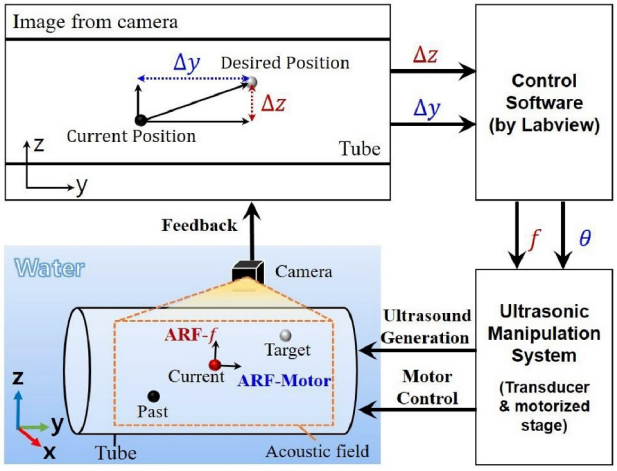

Fig. 6. The illustration of feedback control mechanism for position tracking.

is composed of several components as shown in eqn (8) and (9). P_{iz} and P_{iy} are the initial position of the particle in each direction and P_n is a function indicating the position of the nodes according to the frequency expressed in (7). i_{stage} represents the movement of the stage in accordance with the motorization and $e^{-\tau s}$ represents a delay in the particle movement according to the horizontal operation of the stage. The variables and functions that make up the above equation are found out by repeated simulation and experiment.

Finally, the controller is designed based on the above system equation as follows:

$$F_{ultrasound} = E^{+}(e_z)S_u(\tau) + E^{-}(e_z)S_d(\tau), \tag{10}$$

$$S_u(\tau) = \sin\left[2\pi\left(f_0 + \frac{f_1 - f_0}{T}\tau(t,T)\right)\tau(t,T)\right], \tag{11}$$

$$S_d(\tau) = \sin\left[2\pi\left(f_1 + \frac{f_0 - f_1}{T}\tau(t,T)\right)\tau(t,T)\right], \tag{12}$$

$$I_{motor} = K_p e_y, \tag{13}$$

where $E^{+(-)}(e_z) = \begin{cases} 1(0): & e_z \geq 0, \\ 0(1): & e_z < 0, \end{cases}$ and

$$\tau(t,nT) = \begin{cases} \tau = t - nT: & t \geq nT, \\ \tau = t: & t < nT, \end{cases} (n = 1,\ 2,\ 3\cdots).$$

Here, $S(\tau)$ is the linear sinusoidal sweep signal, f_0 and f_1 are the frequency of start(low) and finish(high), T is the total length of excitation time, and $\tau(t,T)$ is a function that repeats every T, as time progresses.

There are two reasons for selecting a sweep signal as an input signal while designing the controller. The first reason is for smooth motion control of particles. Since the position of the node can be linearly controlled by changing the frequency of the ultrasonic wave linearly, we can drive particles smoothly by incorporating the frequency variation. The second reason is for velocity controllability. Because the sweep time and the sweep range of the input waveform are related to the driving velocity of particles, we can utilize them for different velocity control of micro particles. Therefore, to encounter input frequency, sweep range, and sweep time altogether, we choose a form of sinusoidal sweep signal as control input to the system.

Continuing with the description of the controller, each directional error (e) is obtained by camera image processing, and $E^{+(-)}(e_z)$ denotes switching controller for ultrasonic actuation. The switching point is determined by the sign of the error value in the z-direction. If the error is positive, the current position of the particle is below the desired position and results in the signal $S_u(\tau)$ going up. Conversely, if the error is negative, the signal $S_d(\tau)$ sends the particle downwards. The motor control proceeds through the P controller via position error.

In this study, we have selected f_0 and f_1 to be 800-1300, 900-1500, and 1000-1700 kHz, in the frequency range around 950 kHz, which is the resonance frequency of the transducer. In addition, various variables ranging from 2 to 10 sec were included in T, and the difference in the levitation test results according to each variable was analyzed. Based on the results, we applied each parameter to the visual feedback control experiment [30].

4. EXPERIMENTAL RESULTS

4.1. Experimental setup

The system consists of an ultrasonic driving module and a control equipment. Fig. 7 shows a detailed setup of the system for the whole experiment. The driving module is divided into two parts. One is an ultrasonic transducer that generates ultrasound and the other one is a motorized linear stage that moves the transducer. The ultrasonic transducer used has a resonance frequency of 950 kHz with a diameter of 60 mm. It also has a curvature structure on the ultrasonic wave generating surface to form a focus. The focus was designed 58 mm above the transducer.

As shown in the picture above, this transducer can be moved in the x-y plane by connecting it with a two-axis motorized linear stage. The control unit consists of a function generator (Agilent 33220A) and a high-speed bipolar amplifier (NF HSA4101). The input signal is a sinusoidal wave which is generated by a function generator and transmitted to the ultrasonic transducer through the amplifier at approximately 10 to 25 V. The frequency of the ultrasound is controlled through the LabVIEW program of the PC.

The experiment was carried out by placing the transducer of the ultrasonic driving system described above in a water tank, filling the micro-particle and water to place the circular plastic tube in the focus region of the transducer inside the water tank. The micro-particles were spherical micro-scaffolds (drug delivery carriers) with diameters of 300 μm. In addition, the camera (Microsoft LifeCam) behind the tube was used to provide feedback for automatic

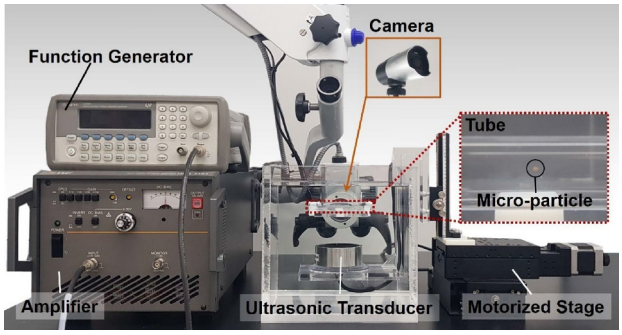

Fig. 7. Experimental setup for ultrasonic actuation.

control of micro-particles within the tube. The captured image from camera is divided into pixel-by-pixel data including particles and tube altogether. Then, the particle position can be calculated based on the reference frame of the tube that is already known by the experimental setup, relatively. However, the camera is not appropriately ready in clinical setting, we need to incorporate other visualization methods for particle position recognition in the future.

4.2. Levitation

The most important aspect of driving particles in the tube is controlling the input signal to the ultrasonic transducer in the z-direction. For smooth and precise movement of the micro particles, we used a sinusoidal wave signal that swept a specific range of frequencies and time intervals. The first experiment involved performing z-directional position control of a micro-particle using the changes in ultrasonic properties in a tube immersed in a water bath. Based on this experiment, we compared the change in pressure nodes and micro-particles' position according to the frequency change of the input signal. Hereafter, the change in the micro-particle velocity was observed by varying the setting parameters of the signal, and the frequency of the input signal and the change in the target position with time were analyzed.

Fig. 8 shows the quantitative data analysis according to the above-mentioned experiment. Fig. 8(a) shows the results of the simulated node positions of Fig. 4 and the trapping positions of the micro-particles identified by actual experiments. When the positions of the simulated nodes and the trapping positions are compared, it can be confirmed that the errors is within 1 mm but discrepancy exists. In addition to the un-modeled environmental condition of the experiments, this is mainly caused by the phenomena that the ultrasonic intensity and pressure tends to decrease as the operating frequency changes to out of the ultrasonic transducer resonant frequency. In practice, we could observe that the highest pressure is observed at 950 kHz that is the resonance frequency of the transducer in this experiments and the pressure decreases as it goes out of resonant frequency range. This also affects the acoustic radiation force that reduces the force acting against gravity, and consequently, the micro-particles are also dropped down slightly. However, this position difference can be compensated by using the feedback control scheme for particle motion control.

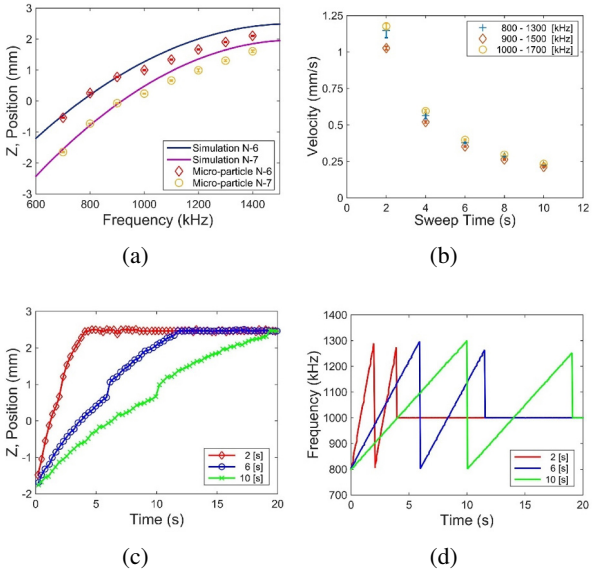

Fig. 8. (a) The positions of micro-particle at Node 6 and 7 with frequency variation by 100 Hz term. (b) The speed in accordance with the frequency range or sweep time of the input sweep signal. (c) The positional change and (d) the frequency change of the signal with time.

Fig. 8(b) shows the result of analyzing the frequency range of the sweep signal and the velocity of the micro-particle according to the sweep time. The faster the sweep time was, the faster the speed was measured. If the sweep frequency was selected with an increased frequency range or a longer wavelength, the speed would tend to be faster. Fig. 8(c) and (d) show the frequency change of the input signal and the position of the micro-particle, respectively, over time. A sine wave swept in the range of 800-1300 kHz was used as the input signal and the frequency of the signal was measured by an oscilloscope. The sweep time was changed to 2, 6, and 10 sec. The micro-particles accelerated with a shorter sweep time and reached the target position sooner. When the input signal swept once at 800-1300 kHz and then back to 800 kHz, the particle jumped slightly in all three cases in which the sweep time was set differently. However, this produced minimal error, making stable control achievable. In addition, high accuracy in position control can be confirmed by comparing the appearance of each micro-particle until it reaches the final target from the initial position. This verifies that the ultrasonic transducer enables precise position control of the micro-particles in the acoustic field in the tube along the z-axis.

4.3. Composite motion control

Fig. 9 shows the results of open-loop driving control for the micro-particle through the ultrasonic driving system in time order according to the method. In Fig. 9(a), the micro-particles are trapped at one node of the stationary wave of 1 MHz inside the tube and move up as shown in Fig. 9(b), when the input frequency is increased. As seen in Fig. 9(c), if the frequency is fixed again, the micro-particles get trapped and move to the right through motorization. If the frequency is lowered, the particles move downwards like Fig. 9(d). This is a key driving method in ultrasonic manipulation, and we have studied the applica-

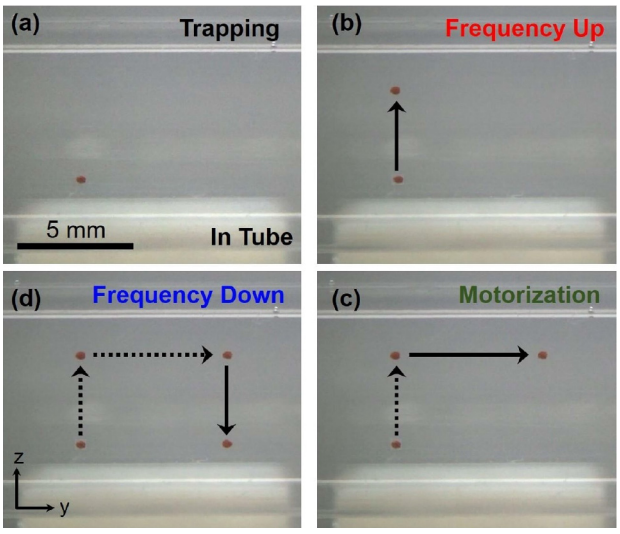

Fig. 9. Proceed in sequence with photos driven by frequency and motor control manually inside the tube.

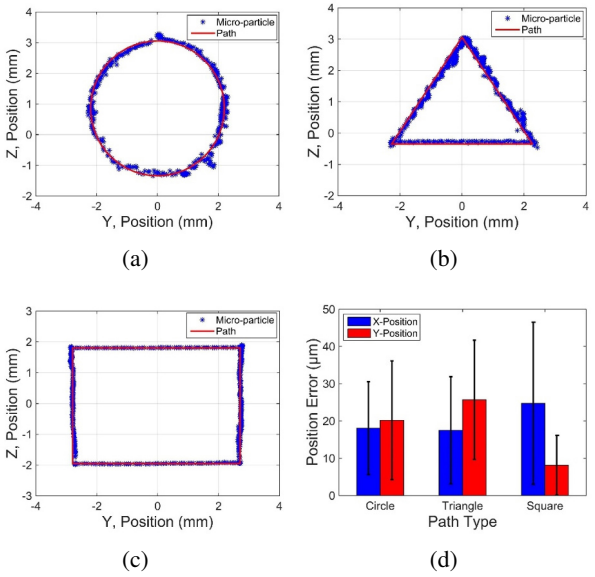

Fig. 10. Results of path automatic control experiment. (a)-(c) Comparison of set path and particle tracking position. (a) circle, (b) triangle, and (c) path of a square model. (d) Absolute position error and standard deviation for each pattern.

tions of control related to it.

We also carried out a feedback control experiment to follow a specific path of a circle, rectangle, and triangle shape as shown in Fig. 10(a)-(c) and Fig. 11.

In Fig. 10, each of the paths represents (a) a pattern of a circle, (b) a triangle, and (c) a square. The microparticles were controlled to follow the set paths, which were operated through the proposed feedback control system. As mentioned above, the control system uses frequency control and motorizing stage simultaneously and is controlled through real-time vision feedback by particle tracking [31]. In the path control experiment, the results include some of the driving instability of the target particles, but the results of successful ultrasonic driving are shown in Fig. 10(a)-(c) in the graph. Fig. 10(d) shows the absolute error and standard deviation for the y and z-positions in each pattern type. The error was compared between each point existing in the planned path and the actual position of the micro-particle, and the error was within 500 μm as a whole. However, when the results shown in the graph are checked, it is seen that microparticles are unstably jumping from their original position in the circle and triangle pattern. It is assumed that this is caused by the difference arising due to acoustic streaming and node position, which in turn is caused by the frequency change of the transducer. Nonetheless, we have shown that even within this unstable point, errors within 1 mm have been demonstrated, and consequently, precise movement control of micro-particles through the ultrasound is possible.

For potential medical applications of microrobots, we performed an *in-vitro* test for manipulation. In the experiments, a plastic circular tube with a diameter of 10 mm and micro-scaffolds with a diameter of 300 μm were used that mimic the no-flow vessel condition. This condition may be available if the procedure incorporates a balloon catheter that blocks flow in a vessel instantly. However, it needs to be validated further in future studies. To implement tissue characteristics, a 6% gelatin solution was hardened outside the tube and wrapped around it with a thickness of 10 mm to make a phantom [32, 33].

Fig. 11(a) and (b) show the tube used for the test with gelatin wrapped on its surface. Inside, there are a number of micro-scaffolds filled with water. The results of the ultrasonic actuation experiments were shown in Figs. 11(c)-(f). It proves that ultrasound can penetrate the gelatin and control the micro-scaffolds through the actuation mechanism. In addition, unlike conventional external actuation systems that use different principles, the results could demonstrate the advantage of trapping ability from ultrasonic actuation. Each photograph shows that the microscaffolds indicated by blue circles could move up, down, and right in the direction of the red arrow by the proposed methods. These results verify the feasibility of this approach for drug delivery and targeting ability of the microrobot which is injected into the blood vessels present in the body.

5. CONCLUSION

In this study, we proposed a position control method through an untethered manipulation mechanism using one ultrasonic transducer and motorized linear stage. We controlled the z-axis position of micro-particles through frequency control of the transducer and added the degree of

freedom through the motorized stage. Also, vision feedback control for automatic control is used to keep track of the pattern. The characteristics of the acoustic field generated inside the tube for this study are confirmed through simulation. Experiments were conducted to verify the concepts and characteristics. The frequency control of a single ultrasonic transducer has shown that to achieve a precise and high level of micro-particle position control, the pressure node that captures it can be relocated by a change in frequency. It has been shown that it is possible to control the driving speed of micro-particles through parameters such as input signal frequency range and sweep time and control movement according to the desired travel route.

However, there are some limitations in this study for practical clinical applications. The first is the problem of mimicking experiments in vessels where a circular tube with a flat wall is used. When we apply it to actual peripheral blood vessels, different characteristics of the ultrasound may be induced in the target region, such as the interference of other media in the body tissues and penetration of ultrasound into the blood vessels. Secondly, we need to further consider blood pressure and flow in vessels. Although balloon catheter and flow blocking agencies are already available, and peripheral venous has a relatively slow flow, we need to consider hemodynamics to extend the applicability of the proposed system.

In conclusion, the feasibility shown in this study depicts a possibility for untethered microrobots, especially in an environment having a shape similar to a circular tube. It can be a useful clinical application in the form of a precise drug delivery tool. Further research will be initiated for the development of a practical wireless microrobot system for drug delivery that enables precise targeting in peripheral blood vessels, which is similar to a circular tube.

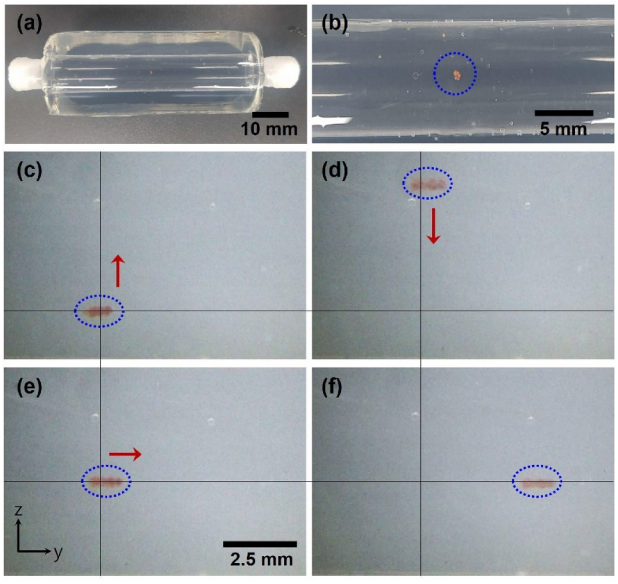

Fig. 11. The results of the In vitro experiment. (a), (b) The experimental tube and the micro-scaffolds inside it. (c)-(f) Manipulating the cluster unit micro-scaffolds with a diameter of 300 μm through the frequency and motor control.

REFERENCES

[1] L. Ricotti, A. Cafarelli, V. Iacovacci, L. Vannozzi, and A. Menciassi, "Advanced micro-nano-bio systems for future targeted therapies," *Current Nanoscience*, vol. 11, no. 2, pp. 144-160, 2015.

[2] F. Soltani, M. K. Khanmohammadi, S. Ghalichi and F. Janabi-Sharifi, "A soft robotics nonlinear hybrid position/force control for tendon driven catheters," *International Journal of Control, Automation and Systems*, vol. 15, no. 1, pp. 54-63, 2017.

[3] H. Choi, K. Cha, J. Choi, S. Jeong, S. Jeon, G. Jang, J. O. Park, and S. Park, "EMA system with gradient and uniform saddle coils for 3D locomotion of microrobot," *Sensors and Actuators A: Physical*, vol. 163, no. 1, pp. 410-417, 2010.

[4] H. Choi, S. Jeong, G. Go, C. Lee, J. Zhen, S. Y. Ko, and S. Park, "Equitranslational and axially rotational microrobot using electromagnetic actuation system," *International Journal of Control, Automation and Systems*, vol. 15, no. 3, pp. 1342-1350, 2017.

[5] G. Go, Z. Jin, J. O. Park, and S. Park, "A Thermo-electromagnetically actuated microrobot for the targeted transport of therapeutic agents," *International Journal of Control, Automation and Systems,* vol. 16, no. 3, pp. 1341-1354, 2018.

[6] D. Baresch, J. L. Thomas, and R. Marchiano, "Observation of a single-beam gradient force acoustical trap for elastic particles: acoustical tweezers," *Physical Review Letters*, vol. 116, no. 2, p. 024301, 2016.

[7] F. Guo, Z. Mao, Y. Chen, Z. Xie, J. P. Lata, P. Li, and S. Suresh, "Three-dimensional manipulation of single cells using surface acoustic waves," *Proc. of the National Academy of Sciences*, vol. 113, no. 6, pp. 1522-1527, 2016.

[8] X. Ding, S. C. S. Lin, B. Kiraly, H. Yue, S. Li, I. K. Chiang, and T. J. Huang, "On-chip manipulation of single microparticles, cells, and organisms using surface acoustic waves," *Proc. of the National Academy of Sciences*, vol. 109, no. 28, pp. 11105-11109, 2012.

[9] A. Marzo, A. Barnes, and B. W. Drinkwater, "TinyLev: A multi-emitter single-axis acoustic levitator," *Review of Scientific Instruments*, vol. 88, no. 8, p. 085105, 2017.

[10] N. F. Läubli, N. Shamsudhin, H. Vogler, G. Munglani, U. Grossniklaus, D. Ahmed, and B. J. Nelson, "3D manipulation and imaging of plant cells using acoustically activated microbubbles," *Small Methods*, p. 1800527, 2019.

[11] C. R. Courtney, C. K. Ong, B. W. Drinkwater, A. L. Bernassau, P. D. Wilcox, and D. R. S. Cumming, "Manipulation of particles in two dimensions using phase controllable ultrasonic standing waves," *Proc. of the Royal Society A: Mathematical, Physical and Engineering Sciences*, vol. 468, no. 2138, pp. 337-360, 2012.

[12] A. Franklin, A. Marzo, R. Malkin, and B. W. Drinkwater, "Three-dimensional ultrasonic trapping of micro-particles in water with a simple and compact two-element transducer," *Applied Physics Letters*, vol. 111, no. 9, p. 094101, 2017.

[13] M. Saito, N. Kitamura, and M. Terauchi, "Ultrasonic manipulation of locomotive microorganisms and evaluation of their activity," *Journal of Applied Physics*, vol. 92, no. 12, pp. 7581-7586, 2002.

[14] Y. Qiu, H. Wang, C. E. Demore, D. A. Hughes, P. Glynne-Jones, S. Gebhardt, A. Bolhovitins, R. Poltarjonoks, K. Weijer, A. Schönecker, M. Hill, and S. Cochran, "Acoustic devices for particle and cell manipulation and sensing," *Sensors*, vol. 14, no. 8, pp. 14806-14838, 2014.

[15] M. Antfolk, S. H. Kim, S. Koizumi, T. Fujii, and T. Laurell, "Label-free single-cell separation and imaging of cancer cells using an integrated microfluidic system," *Scientific Reports*, vol. 7, p. 46507, 2017.

[16] A. Marzo and B. W. Drinkwater, "Holographic acoustic tweezers," *Proc. of the National Academy of Sciences*, vol. 116, no. 1, pp. 84-89, 2019.

[17] M. Prisbrey and B. Raeymaekers, "Ultrasound noncontact particle manipulation of three-dimensional dynamic user-specified patterns of particles in air," *Physical Review Applied*, vol. 10, no. 3, p. 034066, 2018.

[18] Z. Y. Hong, J. F. Yin, W. Zhai, N. Yan, W. L. Wang, J. Zhang, and B. W. Drinkwater, "Dynamics of levitated objects in acoustic vortex fields," *Scientific Reports*, vol. 7, no. 1, p. 7093, 2017.

[19] O. Youssefi and E. Diller, "Contactless robotic micromanipulation in air using a magneto-acoustic system," *IEEE Trans. on Robotics and Automation Letters*, vol. 4, no. 2, pp. 1580-1586, 2019.

[20] J. Li, T. Li, T. Xu, M. Kiristi, W. Liu, Z. Wu, and J. Wang, "Magneto-acoustic hybrid nanomotor," *Nano Letters*, vol. 15, no. 7, pp. 4814-4821, 2015.

[21] A. Marzo, S. A. Seah, B. W. Drinkwater, D. R. Sahoo, B. Long, and S. Subramanian, "Holographic acoustic elements for manipulation of levitated objects," *Nature Communications*, vol. 6, p. 8661, 2015.

[22] A. Marzo, M. Caleap, and B. W. Drinkwater, "Acoustic virtual vortices with tunable orbital angular momentum for trapping of Mie particles," *Physical Review Letters*, vol. 120, no. 4, p. 044301, 2018.

[23] X. Chen, K. H. Lam, R. Chen, Z. Chen, X. Qian, J. Zhang, and Q. Zhou, "Acoustic levitation and manipulation by a high-frequency focused ring ultrasonic transducer," *Applied Physics Letters*, vol. 114, no. 5, p. 054103, 2019.

[24] G. T. Silva and A. L. Baggio, "Designing single-beam multitrapping acoustical tweezers," *Ultrasonics*, vol. 56, pp. 449-455, 2015.

[25] H. Bruus, "Acoustofluidics 7: The acoustic radiation force on small particles," *Lab on a Chip*, vol. 12, no. 6, pp. 1014-1021, 2012.

[26] T. Laurell, F. Petersson, and A. Nilsson, "Chip integrated strategies for acoustic separation and manipulation of cells and particles," *Chemical Society Reviews*, vol. 36, no. 3, pp. 492-506, 2007.

[27] K. Yosioka and Y. Kawasima, "Acoustic radiation pressure on a compressible sphere," *Acta Acustica united with Acustica*, vol. 5, no. 3, pp. 167-173, 1955.

[28] L. V. King, "On the acoustic radiation pressure on spheres," *Proc. of the Royal Society of London. Series A-Mathematical and Physical Sciences*, vol. 147, no. 861, pp. 212-240, 1934.

[29] P. B. Muller, R. Barnkob, M. J. H. Jensen, and H. Bruus, "A numerical study of microparticle acoustophoresis driven by acoustic radiation forces and streaming-induced drag forces," *Lab on a Chip*, vol. 12, no. 22, pp. 4617-4627, 2012.

[30] S. Li, A. Ghasemi, W. Xie, and Y. Gao, "An enhanced IBVS controller of a 6DOF manipulator using hybrid PD-SMC method," *International Journal of Control, Automation and Systems*, vol.16, no. 2, pp. 844-855, 2018.

[31] H. Kang, H. S. Lee, Y. B. Kwon, and Y. H. Park, "A sequential estimation algorithm of particle filters by combination of multiple independent features in evidence," *International Journal of Control, Automation and Systems*, vol.16, no. 3, pp. 1263-1270, 2018.

[32] S. Wang, S. Aglyamov, A. Karpiouk, J. Li, S. Emelianov, F. Manns, and K. V. Larin, "Assessing the mechanical properties of tissue-mimicking phantoms at different depths as an approach to measure biomechanical gradient of crystalline lens," *Biomedical Optics Express*, vol. 4, no. 12, pp. 2769-2780, 2013.

[33] A. Maeva, *High Frequency Shear Wave Imaging: A Feasibility Study In Tissue Mimicking Gelatin Phantoms*, Doctoral Dissertation, 2014.

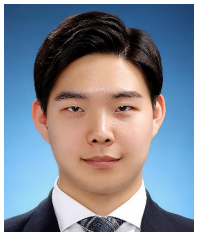

Han-Sol Lee received his B.S. degree from the Department of Mechanical Engineering at Chonnam National University, Korea in 2018. Currently, he is a M.S. candidate in Chonnam National University. His research interests include dynamics and control applications for mecha-nical systems.

Gwangjun Go received his B.S. and M.S. degrees from the Department of Mechanical Engineering at Chonnam National University, Korea, in 2013 and 2015, respectively. Currently, he is a Ph.D. candidate in Chonnam National University and a researcher in the Robot Research Initiative (RRI). His research interests are micro/nanorobots.

Eunpyo Choi received his B.S., M.S., and Ph.D. degrees from the department of mechanical engineering at Sogang University, Korea, in 2008, 2010, and 2015, resepctively. He was a senior postdoctoral fellows in the Dept. of Bioengineering at University of Washington, USA. He is now an assistant professor in the School of Mechanical Engineering at Chonnam National University, Korea. His research interests are BioMEMS and micro/nanorobots for medical approaches.

Byungjeon Kang received his B.S. and M.S. degrees in mechanical engineering from the Chonnam National University, Gwangju, Korea, and a Ph.D. degree in biorobotics from Scuola Superiore Sant'Anna, Pisa, Italy, in 2008, 2010, and 2015, respectively. He is a senior research scientist in the Medical Microrobot Center, Chonnam National University, Gwangju, South Korea. His research interests include microactuator/robot and micro-manipulation for biomedical applications.

Jong-Oh Park received his B.S. and M.S. degrees from the department of mechanical engineering, Korea, and a Ph.D. in robotics from Stuttgart University, Germany, in 1978, 1981, and 1987, respectively. Between 1982 and 1987, he worked as a guest researcher at the Fraunhofer-Institut für Produktionstechnik und Automatisierung (FhG IPA), Germany. He worked as a principal researcher in the Korea Institute of Science and Technology (KIST) from 1987 to 2005, and he was a director of the Microsystem Research Center at KIST from 1999 to 2005. In 2005, he moved to Chonnam National University where he is now a full professor in the School of Mechanical Engineering and a director of the Robot Research Initiative (RRI). His research interests are biomedical microrobots, medical robots, and service robots.

Chang-Sei Kim received his B.S., M.S., and Ph.D. degrees from the Dept. of Control and Mechanical Engineering at Pusan National University, the Dept. of Mechanical Design and Production Engineering at Seoul National University, and the School of Mechanical Engineering at Pusan National University, in 1998, 2000, and 2011, respectively. He was a Research Associate in the Dept. of Mechanical Engineering at University of Maryland College Park, USA He is now an Assistant Professor in the School of Mechanical Engineering at Chonnam National University, Korea. His research interests are dynamics and control applications for mechanical and biomedical systems in the real world.